Journal of Volcanology and Geothermal Research 411 (2021) 107180

Contents lists available at ScienceDirect

Journal of Volcanology and Geothermal Research

journal homepage: www.elsevier.com/locate/jvolgeores

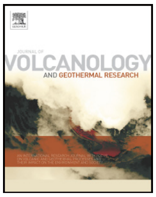

Invited Research Article

Shallow subaqueous to emergent intra-caldera silicic volcanism of the Motuoapa Peninsula, Taupo Volcanic Zone, New Zealand – New constraints from geologic mapping, sedimentology and zircon geochronology

Szabolcs Kósik [a,b,*], Károly Németh [a], Martin Danišík [c], Jonathan N. Procter [a], Axel K. Schmitt [d], Bjarne Friedrichs [d], Robert B. Stewart [a]

[a] Volcanic Risk Solutions, School of Agriculture and Environment, Massey University, Private Bag 11 222, Palmerston North 4442, New Zealand
[b] Horizons Regional Council, Private Bag 11025, Palmerston North 4442, New Zealand
[c] John de Laeter Centre, Curtin University, Perth, WA 6845, Australia
[d] Institute of Earth Sciences, Ruprecht-Karls-Universität Heidelberg, Im Neuenheimer Feld 236, D-69120 Heidelberg, Germany

ARTICLE INFO

Article history:
Received 3 September 2020
Received in revised form 9 December 2020
Accepted 12 January 2021
Available online 19 January 2021

Keywords:
Silicic hydrovolcanism
Zircon
(U-Th)/He dating
U-Th disequilibrium dating
Tuff cone
Lava dome and coulee
Lake Huka

ABSTRACT

Motuoapa Peninsula, located in the southeast of the Taupo Volcanic Centre, New Zealand, is dominated by a silicic pyroclastic cone and overlaying lavas. The pyroclastic succession has not been recognised and studied before, and its thickness and sedimentological characteristics indicate completely different eruption mechanisms than proposed for the other pyroclastic successions within the central Taupo Volcanic Zone. Here, we present the results of field mapping and sedimentological characterisation of accessible pyroclastic deposits, and complement these data with combined U-Th and (U-Th)/He zircon geochronology providing first constraints on the succession's crystallization and eruption history.

(U-Th)/He zircon eruption ages of 77.2 ± 6.3, 81.3 ± 9.2 and 34.5 ± 3.1 ka indicate that volcanic activity in the Motuoapa Peninsula occurred in two distinct eruptive episodes that were separated by ca. 45 kyrs. The earlier rhyolitic eruption at ca. 80 ka is inferred to have commenced in a shallow subaqueous environment. Its lowermost succession includes breccias and tuff breccias sourced from an extruding lava dome by autobrecciation, quench-fragmentation and localised debris flows. With gradual emergence of the growing volcanic pile, explosive hydrovolcanic activity became dominant, constructing an emergent cone by pyroclastic density currents and fall-out. The lack of exotic/accidental clasts, along with an abundance of low-vesicularity rhyolitic juvenile fragments, suggests fragmentation driven by magma-water interaction, which predominantly occurred at shallow depths within the outgassed part of the ascending magma. The frequency and thickness of ash-dominated units increases upwards, suggesting a gradual increase in explosive energy of tephra jets. The final phase of the rhyolitic activity was dominated by emplacement of viscous lava that breached the crater rim and flowed onto the SE sector of the pyroclastic cone. The remnant of the Motuoapa pyroclastic cone, along with the bedded structure of deposits that comprise fallout and surge-dominated units, appears very similar to Surtseyan tuff cones and silicic tuff/pumice cones described elsewhere. A dacitic eruption that produced a nearby lava dome at ca. 35 ka, represents a significantly younger event that occurred after substantial erosion of the earlier pyroclastic cone. The Motuoapa Peninsula deposits most likely record the evolution of a subaqueous silicic eruption, where hydrovolcanism played a fundamental role on subaerial pyroclastic cone formation in a terrestrial environment with abundant surface water availability. The similarities between the environment of the Taupo area today and the area during the Motuoapa activity at ca. 80 ka may provide an analogue model for future subaqueous eruptions in the region.

1. Introduction

The Taupo Volcanic Zone (TVZ, Fig. 1) is the most productive silicic volcanic region on Earth, with 12 caldera-forming and more than 300 low-magnitude silicic eruptions in the past 350 ky (Wilson et al., 2009;

---

* Corresponding author at: Volcanic Risk Solutions, School of Agriculture and Environment, Massey University, Private Bag 11 222, Palmerston North 4442, New Zealand.
E-mail address: szabolcs.kosik@gmail.com (S. Kósik).

https://doi.org/10.1016/j.jvolgeores.2021.107180
0377-0273/© 2021 Elsevier B.V. All rights reserved.

1. Introduction

The Taupo Volcanic Zone (TVZ, fig. 1) is the most productive silicic volcanic region on Earth, with 12 caldera-forming and more than 300 low-magnitude silicic eruptions in the past 350 ky (Wilson et al., 2009; Kósik et al, 2020). During this period at least 3900 km^3 DRE of volcanic material has been produced (Wilson et al., 2009; Gravley et al., 2016; Kósik et al., 2017). Numerous calderas formed during explosive silicic eruptions were filled with water (e.g., Taupo, Rotorua and Okataina Volcanic Centres), but intra-caldera dome-forming eruptions may associated with hydrovolcanism has received little attention. Sudden and abrupt caldera lake level changes and the formation of large lacustrine systems following major caldera-forming silicic eruptions are an integral part of the geological evolution of the TVZ, and post-caldera volcanism within subaqueous conditions is likely expected in the central North Island of New Zealand (Manville et al., 2009; Manville, 2010; von Lichtan et al., 2016). Silicic hydrovolcanic activity has been identified throughout some of the caldera-forming eruptions, such as the ca. 280 ka Ohakuri, the ca. 25.4 ka Oruanui and the 232 AD Taupo events (Smith and Houghton, 1995; Wilson, 2001; Gravley, 2004), along with lower magnitude brief explosive events known from medial to distal products that erupted through the geological record of the Okataina and the Taupo Volcanic Centres (Wilson, 1993; Jurado-Chichay and Walker, 2000). In New Zealand, pyroclastic, cone-forming, silicic volcanism was studied earlier at Puketerata (Brooker et al, 1993; Kósik et al., 2019) and few other silicic pyroclastic cone remnants were identified mostly at Okataina and on Mayor Island (Tuhua) (Houghton et al., 1987; Houghton et al., 1992; Nairn, 2002, Németh and Kósik, 2020b) (Fig. 1). The Okataina structures are often referred to as tuff cones (Nairn, 2002; Kobayashi et al., 2005), however, their stratigraphy and volcanic activity is poorly documented, whereas their topographic positions are not favorable for tuff cone-forming processes that require magma-water explosive interaction in a shallow standing body of water (Németh and Kósik, 2020a). In contrast, paleoenvironmental reconstructions for the time period 200 ka to 25 ka, based on other localities indicate that large parts of present day Taupo area were occupied by large and often deep lakes (Manville and Wilson, 2004, Barker et al., 2020), however, hydrovolcanism was only confirmed for eruptions of silica-poor magmas from this period (Brown et al., 1994). The Motuoapa eruption was most likely initated in a subaqueous environment on the bottom of the southermost part of paleo-Lake Huka (Manville and Wilson, 2004) and the influence of external water in eruptive processes could be subtantial during the subaqueous part of the activity.

In respect of the volcanism of silicic calderas, such as the Taupo volcano, the main focus is often on the climactic super-eruptions producing hundreds to thousands of km^3 volume of volcanic material during the evacuation of magma reservoir, which coincides with the formation of a morphological depression (caldera) due to the subsidence or collapse of the ground surface (e.g. Walker, 1984; Lipman 1997; Cole et al., 2005). The hazards and consequences of such large-volume, but extremely unlikely eruptions overshadow the more frequent smaller events (Kósik et al., 2020), which with random occurrence, great variability of eruption styles, and possible prolonged eruption duration imply serious impacts at local or sometimes regional scales. In contrast with the mitigation strategies for volcanic hazard of caldera-forming eruptions, small eruptions requires complex response plans that taking into account the possible changes of eruption styles in relation to the environmental and economical impacts (Tilling, 1989; Bignami, 2012).

This study investigates the rhyolitic succession of the Motuoapa Peninsula (Fig. 1) including a more than 100 m thick pyroclastic sequence that has not been investigated before. Excluding ignimbrites, the existance of such a thick pyroclastic succession is unique within the TVZ. The sedimentological characteristics and thickness of these deposits indicate their proximity to source vent(s). The pyroclastic succession is exposed only in the high cliffs along the lakeshore created by wave action and tectonic subsidence of the Taupo Rift (Davy and Caldwell, 1998). This study describes the main lithofacies of the pyroclastic succession and lavas of Motuoapa Peninsula with the aim to reconstruct the activity associated with the eruption of degassed rhyolitic magma, and provide time constraints on pre-caldera volcanic activity by means of combined U-Th disequlibirum and (U-Th)/He zircon dating (Schmitt et al., 2006; Danišík et al., 2017). In addition, we attempt to define the most common characteristics of prolonged silicic eruptions that were influenced by shallow standing water bodies.

2. Geological setting

The TVZ is a rifting arc located at the southern end of the Tonga-Kermadec Arc that has been evolving for the past 2 Myrs as a result of oblique subduction of the Pacific Plate underneath the Indo-Australian Plate (Wilson et al., 1984; Cole, 1990; Davey et al., 1995; Wilson et al., 1995; Acocella et al., 2003; Wallace et al., 2004; Spinks et al., 2005; Rowland et al., 2010; Reyners, 2013; Mortimer and Scott, 2020) (Fig. 1). The northern and southern parts of the TVZ are characterised by eruptions of intermediate magmas, whereas the central TVZ is dominated by rhyolitic volcanism, with seven calderas or caldera complexes and hundreds of small-volume volcanoes constructed from predominantly rhyolitic lava and pyroclasts/pyroclastic rocks that formed over the past 350 kyrs (Wilson et al., 1995; Spinks et al., 2005; Gravley et al., 2016;).

Motuoapa volcanism is confined to the pre-25 ka activity of Taupo volcano as suggested by stratigraphy (Leonard et al., 2010), however, due to lack of geochronological data the absolute age of Motuoapa volcanism is not known. Prior to the landscape-changing Oruanui caldera-forming event (ca. 25.4 ka; Vandergoes et al., 2013), during which supereruption of Taupo volcano produced 530 km^3 DRE of magma through the deposition of tens to hundreds of meter thick ignimbrite and widespread tephra fall (Wilson, 2001), the low-lying areas from Reporoa caldera to Taupo were occupied by the ancient Lake Huka (Manville and Wilson, 2004). This paleoenvironmental setting of the Taupo area was similar to the present day Lake Taupo (Manville and Wilson, 2004; Barker et al., 2020). Motuoapa Peninsula is located along the southeast shore of Lake Taupo (Fig. 1). There is a small geothermal system on the east shore of Motuoapa Peninsula (Bibby et al., 1991) where springs are characterised by mature, deep alkali chloride-rich geothermal fluids (Mahon and Klyen, 1968; Murgulov et al., 2016). The basement of the Motuoapa Peninsula is not exposed, but lacustrine deposits (Huka Falls Formation), welded ignimbrite of Whakamaru Group or older rhyolitic lavas may represent as rock units forming its underlying rocks (Davy and Caldwell, 1998; Manville and Wilson, 2004, Leonard et al., 2010). Only rhyolitic lava was identified previously within this area with a mineral assemblage including fayalitic olivine (Ewart et al., 1975; Sutton et al., 1995), however, during a more recent mapping of the area Kósik (2018) identified rhyolitic pyroclastic rocks and an overlying dacitic lava dome in the NE corner of the peninsula (Fig. 1).

3. Samples and methods

During field mapping, the cliffs of the peninsula facing the lake were approached by water. Only the lower parts of the outcrops at the elevation of the lake level were accessible in this manner. Three outcrops consisting of the rhyolitic pyroclastic successions were sampled for granulometry, density analysis and petrography (localities 2-01, 2-05, 3-09; Fig. 1) just above the lake level. Lava samples were collected from five additional locations along the lake shore and one sample (locality 3-01) from the top of the cliffs was collected for petrographic analysis (Fig. 1). Other localities (indicated by blue dots on Fig. 1) were examined by visual observations only. The uppermost sections of the succession were described by high resolution images taken 50-100 m from the cliff face on the lake.

The pyroclastic samples were dry sieved at half phi (ϕ) intervals for grain size, componentry and density analysis. Grain size parameters, such as mean diameter and sorting were calculated using the Gradistat 8.0 software run in Microsoft Excel (Blott and Pye, 2001). Envelope density (D_{env}) measurements of were carried out using a Micromeritics GeoPyc 1360 Envelope Density Analyser at Massey University for 60 lapilli fragments (−3 ϕ and -2.5 ϕ) per sample. The solid densities (D_{sol}) were determined by a Quantachrome Ultrapycnometer 1000 hosted also at Massey University, using N_2 gas as the flowing medium. Bulk vesicularity was calculated by $1-(D_{env}/D_{sol})$ using 2.46 g/cm^3 of average solid density of the rhyolite (Houghton and Wilson, 1989). Textural and petrographical characterisations of samples were determined through optical microscopy of thin sections of lapilli fragments, as well as with a FEI Quanta 200 Environmental Scanning Electron Microscope (SEM) equipped with an energy dispersive X-ray spectroscope (EDAX) for ash fragments (0.5 to 2.5 ϕ) at Manawatu Microscopy and Imaging Centre, Massey University.

Three samples representing lavas of the rhyolite (MO-2) and dacite (MO-3) bodies and lapilli fragments from the rhyolitic pyroclastic deposits (MO-1) were dated by combined zircon U-Th disequilibrium and (U-Th)/He dating approach summarized in Danišík et al. (2017) to constrain crystallization and eruption history. The samples were split into 3-5 cm large fragments some of which were submitted to Labwest Minerals Analysis Pty Ltd (Perth, Australia) for trace element analysis by solution ICPMS in order to determine the whole rock

Th/U values that are required for calculating zircon-melt U-Th model ages and for ZDD corrections (Danišík et al., 2017). The remaining rock fragments were separated for zircon picking following a standard workflow for heavy mineral separation at John de Later Centre, Curtin University, Australia. The procedure included disaggregation by SelFrag, magnetic and heavy liquid separation, and hand-picking under a binocular microscope. Zircon crystals were then rinsed in cold 40% HF for 3 min to remove the adherent glass and submitted to the HIP Laboratory at the Institute of Geosciences, Heidelberg University (Germany), for U-Th disequilibrium analysis in order to constrain crystallization ages that are required for the disequilibrium correction of (U-Th)/He data (Farley et al., 2002; Schmitt et al., 2006).

For U-Th disequilibrium analysis, zircon crystals selected based on size and shape were pressed into indium (In) metal with unpolished crystal faces exposed at the surface, coated with a conductive layer of gold and analysed using secondary ionization mass spectrometry (SIMS) with the Heidelberg CAMECA IMS 1280-HR ion microprobe. Isotope analyses of individual zircons were performed following the protocols described in Friedrichs et al. (2020). After the SIMS analysis, zircon crystals were wiped with methanol and soft tissue to remove the gold coating, plucked out from the In mount, and dated by (U-Th)/He methods at the Low-Temperature Thermochronology Facility at John de Laeter Centre, Curtin University, following the procedures described in Danišík et al. (2012; 2020). The raw (U-Th)/He dates were corrected for alpha ejection after Farley et al. (1996) assuming a homogeneous distribution of U and Th. Alpha ejection corrected (U-Th)/He ages were corrected for disequilibrium using MCHeCalc software (Schmitt et al., 2010). The eruption age for each sample was calculated from the disequilibrium corrected (U-Th)/He dates as a weighted mean using Isoplot 4.15 Excel add-in (Ludwig, 2012).

4 Field observations, stratigraphy and facies architecture of the Motuoapa Peninsula

4. 1 Geomorphology and stratigraphy

The Motuoapa Peninsula is bounded by 30-100 m high cliffs facing toward the lake. In contrast, the southern side is characterised by gently sloping areas with a 6-10 m high escarpment that are inferred to be the result of wave cut erosion at lake levels that were the same as today or slightly higher (Fig. 1). An approximately north-south striking normal fault system with an *en échelon* pattern at the south runs across the peninsula, displaying about 16 m vertical movement on the west side and bounding an approximately 200 m wide graben. West of the graben, the terrain slopes from the high areas in the north (top of the cliff faces) to the lower areas in the south by an average of 5-6°, whereas the eastern graben bounding fault runs across a distinct raised ovoid structure in the north with steep-sided (~40°) slopes and a northwardly breached depression in its centre. Slope aspects indicate that a small portion of the lower western flank of the structure remained intact west from the graben (Fig. 1). The gently-sloping terrain in the south part of the peninsula displays one major and two minor slope breaks at elevations of 391, 382.5 and 377 m that are most likely related to the high stand of Lake Taupo developed after the 232 AD caldera-forming eruption of Taupo volcano (Wilson and Walker, 1985; Manville et al, 1999).

Three major stratigraphic units were identified from our sampling on the Motuoapa Peninsula. Stratigraphically, the lowest is a rhyolitic pyroclastic succession (“a” on Fig. 1) with coarse tuff breccia, cross-bedded tuff and lapilli tuff exposed in the cliffs of the northern part of the peninsula (Fig. 1). These deposits are at least 110 m thick in the north-facing cliffs, but only 10-20 m pyroclastic deposits are visible above the lake level along east- and west-facing cliffs (Fig. 1). The pyroclastic sequence is overlain by rhyolitic lava ("b" on Fig. 1), the maximum thickness of which is in the northwest corner of the peninsula, where just over 100 m is exposed between lake level (357 m) and 465 m (locality 3-01 on Fig. 1). The lava appears to thin southward with a measured thickness of 60-65 m at locality 2-03 (Fig. 1). The third stratigraphic unit ("c" on Fig. 1) is a dacite lava (~68% SiO_2) (Kósik, 2018). The dacitic structure has experienced minor erosion compared to the earlier edifce composed of rhyolitic pyroclasts and lavas.

Based on sedimentological observations, six rhyolite lithofacies were distinguished. Three of which were identified as pyroclastic products of stratigraphic unit a and three relate to effusively emplaced lava (stratigraphic unit b). The dacite is only recognised as coherent lava.

4.1.2 Pyroclast characteristics

Pyroclastic fragments are dominantly angular coarse ash and lapilli. Lapilli-sized fragments are characterised by a wide range of bulk vesicularities of up to 56 vol%, with an average of about 30 vol% (Figs. 2-3), along with vitric groundmass, which often exhibits perlitic texture in microscopic scales. Vesicles in lapilli-sized fragments exhibit usually elongated or twisted geometries. Only one well-cemented mostly sumberged lapilli tuff layer sampled at locality 3-09 (Fig. 1) contains pumiceous clasts of up to 1 cm in size that have highly vesicular cores with chilled, vesicle-free rinds (Fig. 2d). Fragments of vitric ash fractions are also characterised by a wide range of vesicularities (Fig. 2a). Most of these fragments are characterised by blocky, angular (or subangular) shapes with uneven distribution of predominantly elongated and bending vesicles (Fig. 2b). The edges of the fragments traverse the vesicles randomly with common surficial cracks (Figs. 2a-c) having attributed to explosive magma-water interaction and resulting fragmentation (van Otterloo et al., 2015). Blocks are more common in the lower part of the succession and are very similar to lapilli fragments in terms of texture and density. Almost all lapilli and block/bomb fragments are classified as dense juvenile pyroclasts (White and Houghton, 2006) having porphyritic flow-banded textures with glassy groundmass (Kósik, 2018). Results of grain-size analysis show the poorly sorted nature of the sampled pyroclastic deposits (e.g., grain size parameters of locality 2-05; Figs. 4h and 5).

4.1.3 Pyroclastic lithofacies (stratigraphic unit “a”)

Clast- to matrix-supported tuff breccia lithofacies (Ex-1) is restricted to the lower 10-15 m of the NW-facing cliffs, between localities P4 and P6 (Fig. 1). Ex-1 lithofacies consists of different packages of reversely, normally, or non-graded, poorly sorted domains with thicknesses ranging from 30 cm to at least 5 m, and are characterised by diffuse and rapid lateral variations. Lensoid features are common (Fig. 4e). Non-graded packages are massive or display diffuse or weak stratification (e.g., Fig. 4f). Due to discontinuous exposure, lateral textural variations could not be evaluated between P4 and P6 (Fig. 1). Strong silica cementation of the deposits was observed at 2-02 (Figs. 4d-e) (Fig. 1). Deposits are dominantly characterised by open framework (Figs. 4d-e), but some parts resemble matrix-supported structures (Fig. 4f). The matrix is predominantly composed of juvenile coarse ash. Larger-sized juvenile pyroclasts (up to ~50 cm), mostly angular and subangular, are characterised by variable vesicularities up to 56% with aligned vesicles. Strata dip to 20-25° SSE at locality 2-02 (Fig. 1). Upper and lower contacts of lithofacies Ex-1 with other lithofacies are obscured.

Interpretation: The shape and vesicle textures of fragments of lithofacies Ex-1 (Figs. 4d-e) suggest a source from a growing lava dome. The sedimentological features of thick massive to crudely bedded parts are very similar to deposits of block-and-ash flows. The easterly dip direction at locality 2-02 and the orientation of the common lensoid shape of beds indicate that the cliffs are generally perpendicular to the transport direction. The lack of medium and fine ash could be either the result of restricted clast-clast collison process or delayed and spatially different deposition of fine ash relative to the coarser materials (White et al., 2003). As the vesicularity is usually low, the fragmentation of the lava dome may have occurred passively (Scott et al., 2003) or driven by steam explosions due to water drawn into the opening fractures of the dome's carapace (White et al., 2003). Such an activity usually produces debris flows in subaqueous environment or subaerially block-and-ash flows, debris flows and granular flows (Calder et al., 2002).

Bedded lapilli tuff lithofacies (Ex-2) comprises two types of alternating layers (A and L) of loose material (Figs. 4h-l). Volumetrically, matrix- to clast-supported lapilli tuff (L) is the more significant and characterised by massive to crude bedding, poor sorting and that are reverse, normal or lack of grading. Thicknesses range from few centimetres to about 1 m. At lower stratigraphic levels the beds are thicker and contain lesser amounts of ash (Fig. 4h) than at higher levels in the sequence (Figs. 4k-l). Sampled lower sections of L-beds are dominantly composed of juvenile coarse ash to coarse lapilli with angular fragments up to 15-20 cm in diameter. The analysis of a sample from locality 3-09 (Fig. 1) has an average grain size of 3.8 mm (-1.95 ϕ). The typical grain size distribution of L-beds is plotted (Fig. 4h inset) and indicates a lack of fine ash in these pyroclastic beds. Bulk vesicularity of lapilli fragments yields an average of ~ 30 vol% (up to 56 vol%) based on envelope density measurements (Fig. 3). Another type of beds (A) is characterised by sub-cm to ~15-cm-thick, poorly sorted, matrix-supported, cross-stratified, diffusively bedded and occasionally undulating ash-rich successions. The appearance of A-beds at lower stratigraphic levels is often more diffuse and thinner (Fig. 4h) than is visually observed in the higher levels of the cliffs. Based on visual observations of the sequence at higher stratigraphic levels, ash-rich beds sometimes display significantly lateral changes in thickness. Soft sediment deformation is present but not widespread. Bomb sags or distortions beneath block-sized fargments are rare and limited to A-beds. Lithofacies Ex-2 crops out at the lake level at localities 3-09, 2-01, 2-05, south from P3 (Fig. 1) and along the entire pyroclastic sequence at higher stratigraphic levels. The thickness of the lithofacies exceeds 100 m.

Interpretation: Lithofacies Ex-2 is inferred to be the result of two different processes operating simultaneously or alternating. The large thickness of the deposits indicates the prolonged nature of the corresponding eruptive phase. The vesicularity and grain size and shape properties of examined fragments rule out decompression-driven magmatic fragmentation, which requires at least 75% vesicularity as an average of ash fragments (Houghton and Wilson, 1989), whereas Vulcanian pyroclasts often indicate similar low average vesicularities (Giachetti et al., 2010) to what observed at Motuoapa. However, based on the thickness of the Ex-2 lithofacies and the size of edifice made-up by these pyroclastic deposits, we ruled out the dominance of Vulcanian-style activity. The generally coarse nature, along with the lack of ash fragments under 3 ϕ at L-beds suggests these deposits formed far from the effective magma-water interaction required for sensu stricto phreatomagmatic eruption (Kokelaar, 1983; Wohletz and Sheridan, 1983). Grain size distribution is similar to proximal fall deposits of other hydrovolcanic eruptions with available granulometric data (Fig. 5). In contrast, during the formation of A-beds the fragmentation was more effective. The frequency and thickness of A-beds towards higher stratigraphic levels indicates more efficient fragmentation, which can be attributed to the decreasing availability of external water. L-beds are interpreted to represent proximal deposits sourced from tephra fall of dense tephra jets and low plumes relating to the periods of an eruption style similar to those documented for basaltic Surtseyan eruptions (Kokelaar, 1986; Wohletz and Sheridan, 1983). The cross- and dune-bedded A-beds point towards a pyroclastic density current (PDC)/base surge origin. Deposition from low-energy base surges was most likely related to the collapse of tephra jets. Ballistically ejected larger fragments were also linked to these more energetic events. Cross-stratification and undulation of A-beds evidence subaerial deposition (Carey et al., 1996; Cas and Wright, 1988; Freundt, 2003); however, the diffuse fine-grained layers that appear near the current lake level might have been deposited under water by turbidity currents or from suspension (Cas and Wright, 1988).

Alternatively, the A-beds could also be interpreted as a tail of short run-out PDCs deposited around the active vent (e.g. Dorozno et al., 2010; Dorozno 2012; Valentine et al., 2017) supported by the unsorted nature of the deposits, their quick bedding variations in short distances and cross stratification. While this might work for explaining the lower part of the section, the upper part shows a regular pattern inconsistent with depositions of unsteady and irregular processes. Coarse-grained and angular lapilli and block-rich deposits commonly associated with ballistic curtain deposition when cratering explosions clear the vent in a blast-like fashion (Graettinger et al., 2015; Valentine et al., 2015; Graettinger and Valentine, 2017). Such eruption creates a curtain-like shower of pyroclast mixtures of great size variability commonly falling into the freshly deposited proximal PDC deposits derived from a penecontemporaneous eruptive event. While this model cannot be ruled out completely, ballistic curtain deposits normally represent far better-defined horizons in a tuff ring that are irregularly distributed across the entire section. Our observations, however, show far more gradual vertical facies changes that are consistent with an eruption where similar and continuous processes acted while some factor controlling fragmentation changed gradually.

This is more in line with gradual changes of fragmentation efficiency than with volcanic conduit or crater dynamics. In reality, it is likely that we are dealing with a combination of these three processes at the same time, however, our current observation resolution prevents more refined interpretation.

Chaotically-arranged tuff and tuff-breccia lithofacies (Ex-3) is only recognised at P3 within the lower 5 m of cliffs above lake level (Fig. 1). It consists of a chaotic arrangement of two types of rocks exhibiting Ex-1 and Ex-2 lithofacies. The majority of the lithofacies consists of a disorganised subfacies that is spatially quickly changing (on the meter scale) between clast and matrix supported unlithified tuff-breccias. Weathering has produced random discoloration patterns in colours from ochre to reddish-brownish. Some parts of the tuff-breccia display discontinous, weak stratification, which is interrupted by vertical and subvertical structures. The contacts are usually diffuse with vertical structures distinguishable by contrasting discoloration with its neighbourhood. In places the lithofacies is characterised by a subfacies having stratified beds floating within a coarser matrix. The beds consist of poorly sorted, crudely stratified lapilli tuff and cross-bedded tuff; identical to lithofacies Ex-2. The contacts between the two subfacies are accentuated by differences in grain size and visual attributes across the section (Figs. 4a-c).

Interpretation: The discoloration of the deposits is interpreted to reflect hydrothermal alteration where the distinguished vertical zones could represent pipe structures relating to gas escape. The chaotic nature of the breccia-dominated subfacies exhibit features consistent with a churning process (McClintock and White, 2006). The tilted rafts (bedded subfacies) are identical to Ex-2 lithofacies were most likely sourced from the crater walls by slumping to a depression, suggesting Ex-3 lithofacies formed during or after the formation of Ex-2 lithofacies. These features are common in a vent or intracrater facies of a “wet” vent (Ross and White, 2006; White and Ross, 2011; Ross et al., 2017).

4.1.4 Effusive lithofacies of rhyolite (stratigraphic unit “b”)

Vertically jointed coherent rhyolite (Ef-1) exhibits vertical or steeply lake-ward leaning flower-like irregular columns of coherent lava. Horizontal fractures are rare and usually discontinuous. Columns are between 5 and 15 m wide. The vertical-subvertical jointing of lava intersects the coarse breccias at the base of the exposed sequence but fails to cut the overlying bedded pyroclastic sequences. There is a sharp contact between the vertically jointed lava and the horizontally stratified pyroclastic beds (Fig. 6a). Lava sampled from the top of the cliffs (locality 3-01; Fig. 1) has a strong perlitic texture. This lava lithofacies only appears along a 150 m section of the cliffs at locality P4 (Fig. 1).

Interpretation: Lithofacies Ef-1 is characterised by a columnar fracture network and interpreted as a proximal coherent-lava facies , with features inferred to have developed in response to shearing and relatively slow cooling (Bonnichsen and Kauffman, 1987; Hetényi et al., 2012). The restricted extent of this lava type, the near vertical nature of the contact with the pyroclastic beds, together with the geomorphic characteristics of the peninsula imply the position of the vent area at the position of this lithofacies. The flower structure jointing of lava is similar to crater/vent infills observed in other mafic and silicic monogenetic volcanoes (e.g., Lexa et al., 2010).

Flow-banded coherent rhyolite (Ef-2) lithofacies are characterised by a horizontal/subhorizontal system of sheet joints parallel to the flow laminae (Fig. 6b). The thickest successions are at locality P2 (Fig. 1) where they display pronounced sheet jointing.

Ramp structures and tension cracks are common where lithofacies Ef-2 transitions to lithofacies Ef-3 (Figs. 6c, e-f). The lava is typically dense, glassy to microcrystalline, with rare layers having coarsely vesicular pumiceous textures. Flow-banded rhyolite lava appears between localities P2 and 1-01, along the main fault that dissects the peninsula, and at locality 2-06 (Fig. 1). Spherulitic lavas were sampled at localities 2-03 and 2-06 (Fig. 1). Along the west shore the lava dips 10-15° SSW.

Interpretation: Ef-2 is interpreted as the internal part of a coulee/flow. The dip directions suggest flow to the south along the west shore (Fig. 1).

Monomictic breccia (Ef-3) is characterised by poorly sorted, clast-supported texture, lacking an ash matrix. This lithofacies gradually transitions from coherent lava with ramp structures through jigsaw-fit and clast-rotated textures to massive breccia (Figs. 6c-f). The proportion of vesicular fragments is the greatest within the most brecciated parts of the unit (Fig. 6b). Lava breccias appear along the lake shore, mostly between localities 2-03 and 1-01 (Fig. 1), but a few metre-sized enclaves of brecciated lava were also found within the flow-banded parts.

Interpretation: Ef-3 lithofacies, aside from the small enclaves within the coherent lava, represents near flow front or the base facies of the coulee with ramp structures and autobreccia. We envisage its emplacement and morphological features similar to the Newberry Flow, South Sister volcano or Big Obsidian Flow, Newberry volcano, USA (Anderson et al., 1998; Fink and Anderson, 2017).

4.2 U-Th zircon crystallization ages and (U-Th)/He zircon eruption ages

Samples MO-1 (Ex-2 lithofacies) and MO-2 (rhyolite lava) yielded indistinguishable model zircon-melt U-Th ages with the majority ranging between ca. 85 and 140 ka (Fig. 7; Appendix

1). The youngest U-Th zircon crystallization ages within these populations constrain the eruption age to ≤ 85 ka. Average isochron ages anchored by the measured Th/U whole rock composition for samples MO-1 and MO-2 are 116.6 ± 9 ka (2σ; MSWD = 1.15; n = 14) and 105.3 ± 7 ka (2σ; MSWD = 0.65; n = 17), respectively. Sample MO-3 (dacite lava) yielded significantly younger model U-Th ages ranging between ca. 35 and 80 ka and an isochron age of 58 ± 4 ka (2σ; MSWD = 2.34; n = 20) (Fig. 7; Appendix 1). Although the elevated MSWD value and shape of the probability density function (Fig. 7) may suggest a presence of multiple age populations, principle component analysis by using "auto" mixture model implemented in DensityPlotter 7.3 (Vermeesch, 2012) revealed only one significant component in the dataset. Therefore, the U-Th age distribution is considered unimodal and broad. The youngest U-Th zircon crystallization ages constrain the maximum age of eruption to ca. ≤ 35 ka.

(U-Th)/He results are summarized in Table 1. The weighted average (U-Th)/He ages for eight replicates per each sample are: MO-1 – 77.2 ± 6.3 ka (95% confidence interval (CI); MSWD = 1.16); MO-2 – 81.3 ± 9.2 ka (95% CI; MSWD = 2.1); MO-3 – 34.5 ± 3.1 ka (95% CI; MSWD = 1.01). These ages are interpreted to represent the time of eruption (Danisik et al., 2017) and confirm the observations based on U-Th zircon crystallization ages: Samples MO-1 and MO-2 revealed statistically indistinguishable age populations of single grain (U-Th)/He ages and eruption ages that overlap within analytical uncertainties. Therefore, these samples can be interpreted as belonging to one volcanic event. Combining both samples, the weighted average (U-Th)/He age is 79.6 ± 5.5 ka (95% CI; MSWD = 1.6; n = 16), which is our best approximation of this volcanic event. In contrast, sample MO-3 yielded a significantly younger eruption age (34.5 ± 3.1 ka) which post-dates the previous volcanic event by ca. 45 kyrs. The 34.5 ± 3.1 ka eruption age is also older than the 25.4 ka Oruanui event, which is in agreement with the stratigraphic position of of Motuoapa samples with respect to Oruanui deposits (Leonard et al., 2010).

In all three samples, the oldest U-Th zircon crystallization ages predate their eruption age by <100 kyrs and, on the other hand, the youngest U-Th zircon crystallization ages overlap within uncertainty with the corresponding (U-Th)/He zircon eruption age.

5. Discussion

5.1 Fragmentation and eruptive styles

The interpretion of eruptive styles and related transport and depositional processes are usually based on pyroclast dispersal patterns and characterisation of pyroclastic deposits including bedforms, grain size parameters and componentry. In this study, direct measurements were limited, most exposures were characterised by high resolution images taken from distance. Our interpretation relies on the observed structures of pyroclastic sequences, with the L-beds of Ex-2 yielding most of the data. A-beds and L-beds of Ex-2 lithofacies (bedded lapilli tuff) encompass at least 100 m thick proximal tephra successions, indicating that the eruptive phase was persistent but fluctuated in time. Finer grain size characteristics of A-beds of Ex-2 lithofacies are interpreted to be indicative of a more energetic fragmentation than in eruption of L-beds. Alternatively, the two bed sets could also represent two size populations separated during transportation. The observed cross stratification and weakly developed dune-bedding in A-beds indicate a lateral emplacement mechanism (e.g. by PDC). The grain size distribution of L-beds (Fig. 5) is consistent with a proximal fall-dominated origin, similar to the proximal fall beds of the phreatomagmatic Puketerata eruption (Kósik et al., 2019) (Fig. 8). Their grain size properties are also comparable to the Surtseyan fall beds of North Head volcano, AVF (Agustin-Flores et al., 2015) (Fig. 5). Such fall-dominated pyroclastic successions, having abundant dense fragments, have not been reported for silicic volcanic activity in the central TVZ, thus it is worth to compare these deposits with other well-studied magma-water interaction dominated volcanic eruptions, for example phreatoplinian, phreatomagmatic and Surtseyan activity from New Zealand (Fig. 8).

The observed broad vesicularity range (2-56 %) and the abundance of poorly vesicular fragments are typical of end-member hydrovolcanic eruptions (Houghton and Wilson, 1989), but also observed for pyroclasts at other dome-forming eruptions, such as Chaos Crags, California (Heiken and Wohletz, 1987) and Puketerata, New Zealand (Kósik et al., 2019). The dominant highly deformed vesicle shapes and general low vesicularities of fragments of L-beds suggest bubble collapse, indicating a permeable magma undergoing significant open system degassing before fragmentation (Burgisser and Gardner, 2004; Mongrain et al., 2008; Noguchi et al., 2006). Vesicle shapes in ash fragments are identical to bubbles found in lapilli fragments and flow-banded lava. This, together with the absence of non-juvenile fragments suggest explosive eruption breaking apart shallow-outgassed carapace causing extensive fragmentation of the extruded lava. In contrast, the unique inflated pumice clasts found near the contact between lithofacies Ex-1 and Ex-2 have vesicle-free rinds and probably represent non-degassed magma from the more internal part of the ascending magma column (Fink et al., 1992; Giachetti et al., 2010). Degassing and volatile exsolution from magma make vesicles, implying that the clast exteriors are not degassed (e.g. Mueller and White, 1992), and if pristine, that glass would have high volatile content. This further implies that the glassy rinds were quenched sufficiently to prevent further exsolution at pressures high enough to have held the volatiles in the melt. The rinds were quickly chilled upon contact with water or watersaturated air, whereas cores were syn-eruptively inflated. Similar textures are common within products of submarine eruptions and in breadcrust bombs produced during Vulcanian eruptions (Wright et al., 2007; Giachetti et al., 2010; Duraiswami et al., 2019; Murch et al., 2019). The observed amoeboid shapes of vesicular juveniles were also documented for subaqueous fire-fountains (e.g., Mueller and White, 1992). Angular and blocky shapes and quenching cracks of vitric ash are similar to those decribed in other studies and are attributed to phreatomagmatic origin (e.g., Heiken, 1972; Sheridan and Wohletz, 1983; Heiken and Wohletz, 1987; Büttner et al., 2002).

The ~100 m thickness of Motuoapa's proximal ejecta corresponds well with the morphometric parameters observed in basaltic tuff cones (e.g., Wohletz and Sheridan, 1983; Verwoerd and Chevallier, 1987). The presence of some pumice fragments in these tuff/pumice cone volcanoes indicates the erupting magma had, at least at times, a high gas content, but the limited dispersal of the pyroclastic fragments indicates relatively low-energy fragmentation and explosions. The growth of tuff/pumice cones is often accompanied by the extrusion of obsidian lava flows, and sometimes blocks of obsidian lava are interbedded with pumice layers (Kobayashi, 1982; Dellino and La Volpe, 1995; Cousens et al., 2003; Jensen et al., 2009; Shea et al., 2017). The fallout, pyroclastic surge and small-scale pyroclastic flow deposits of the rhyolitic Monte Pilato cone, Lipari (Italy) (Dellino and La Volpe, 1995), suggest that various types of fragmentation take place during the development of emergent pyroclastic cones. Based on image analysis of particle morphology, Dellino and La Volpe (1995) observed features of magmatic fragmentation for a generation of pumiceous fallout layers from Monte Pilato, whereas the ash beds indicate features more typical of hydrovolcanic fragmentation. The paleoenvironment during the formation of Central Pumice

Cone (Jensen et al., 2009) also suggests at least some degree of magma-water interaction. The pyroclastic beds of the trachytic Puʻu Wa awa cone (Hualālai volcano, Hawaii) appear very similar in many aspects, such as granulometry and stratigraphy to the Motuoapa sequence. However, the Puʻu Wa awa cone sequence is inferred to have been emplaced by eruptions similar to violent Strombolian to Vulcanian activity triggered by conduit processes without substantial interaction with external water (Shea et al., 2017). Besides the pumiceous fragments of Puʻu Wa awa, which may represent magmatic volatile-driven fragmentation (Houghton and Wilson, 1989), the vesicularity range of fragments with other textures (Shea et al., 2017) is very similar to that observed at Motuoapa. The formation of tuff/pumice cones that are characterised by peralkaline compositions is also often explained by magmatic explosive eruptions of Strombolian and Hawaiian style (Houghton and Wilson, 1989; Orsi et al., 1989), but recently examined pyroclasts from pumice cone deposits of Aluto caldera (Main Ethiopian Rift) suggest pumice cone eruptions may be associated with wide-spread tephra fallout and column-collapse-type PDCs likewise in Plinian activity (Clarke et al., 2019). In contrast, our study suggests the dominance of hydrovolcanic fragmentation during the emergent stage of tuff cone formation similar to fragmentation during basaltic Surtseyan eruptions (White and Houghton, 2000). The common feature for each of the silicic tuff cone-forming eruptions described above is the presence of an extruding lava body excavated by explosive activity producing fragments with a wide range of vesicularities and minor accidental lithics (Houghton and Wilson, 1989; Shea et al., 2017; Colombier et al., 2018). This suggest that silicic pumice/tuff cones might be formed by the dominance of strikingly different eruption styles, where the efficiency of vesiculation and the influence of magma-water interaction on fragmentation may vary significantly.

5.2 Reconstruction of the magmatic history of the Motuoapa Peninsula with implications for the broader Taupo area

U-Th zircon age populations in all three samples are characterized by unimodal probability and kernel density distributions with a major peak at ca. 110 ka (MO-1 and MO-2) and 60 ka (MO-3), whereas ages are always within <60 kyrs of the eruption without any anomalously old ages (Fig. 7). It is also noteworthy that the oldest U-Th zircon ages from sample MO-3 are younger than the eruption age of MO-1 and MO-2 samples. These observations may imply that the investigated crystals are autocrysts formed during two distinct magmatic phases – the first commenced at ~140 ka and produced MO-1 and MO-2 zircon crystals for ~60 kyrs until they erupted at ca. 80 ka, whereas the second initiated after the 80 ka eruption and produced MO-3 zircon crystals until their eruption at ca. 35 ka. All U-Th zircon crystallization ages combined also suggest a continuous presence of magma in the Motuoapa magma system between ca. 140 ka and 35 ka. Geographic proximity of samples and the absence of anomalously old U-Th ages suggest that all three samples are rhyolites from a common xenocrystic or antecrystic zircon devoid magma reservoir.

The ca. 110 ka major peak in the U-Th age spectrum predates the main zircon crystallization period of the main Taupo system which occurred at ca. 86-95 ka (Charlier et al, 2005; Wilson et al., 2016). The ca. 80 ka age of rhyolitic eruption and the ca. 60 ka peak recorded by zircon from the dacite are outside of the main zircon crystallization periods of the Taupo magma reservoir according to what has been recorded by zircons from eruption products of the Oruanui event (Wilson et al., 2016). Interestingly, the 45 ka Tihoi eruption (Barker et al., 2014) indicates a bimodal zircon model-age spectrum with peak values similar to the two Motuoapa eruptions (Charlier et al., 2005). The age of the dacite eruption roughly overlaps with a second zircon crystallization maximum suggested by zircons from the Oruanui pumice (Wilson et al., 2016). The zircon crystallization similarities between the two spatially and temporally separated small-volume eruptions (Tihoi and Motuoapa) suggest that these recharge events could have been significant and more than local. In contrast, the Oruanui eruption revealed a wide range of zircon crystallization with peaks at different times (Charlier et al., 2005) suggesting heterogeneity and limited interconnectivity between magma reservoirs beneath Taupo volcano before ca. 40 ka.

The ca. 80 ka eruption recorded by MO-1 and MO-2 samples was a subaqueous silicic eruption which initiated within a lake that most likely represented one of the southernmost parts of ancient Lake Huka. Early activity was predominantly effusive, producing a subaqueously deposited pile of breccia due to the destruction of a growing lava dome. Volcanic activity gradually changed to an emergent stage as the subaqueous environment became shallow enough to enable more energetic explosive magma-water interaction (Reynolds, 1980; Cas et al., 1990). The resulting approximately 100 m thick sequence is characterised by the alternation of pyroclastic surge-dominated and pyroclastic flow and fallout-dominated pyroclastic units. During the final stage of activity, the vent area of the resulting pyroclastic cone became isolated from lake water and effusive activity resumed. The crater was filled by lava, which breached the south-southeast sector of the tuff cone and descended on the slope forming a ~60 m thick coulee (Figs. 1 and 9). This coulee resembles morphological and textural similarities to the Rocche Rosse Flow, Lipari, Italy (Dellino and La Volpe, 1995).

Erupted volume calculations based on a 1 m LiDAR DEM yielded 0.267 ± 0.014 km^3 total dense rock erupted volume for the rhyolitic activity (Kósik, 2018) which is roughly shared equally by the pyroclastic cone building and late stage effusive deposits. Based on Holocene examples for average effusion rates (10-20 m^3/s) at eruptions with degassed silicic magmas (Yokoyama, 2005, Tuffen et al., 2013) the rhyolitic activity of Motuoapa may have been lasted from a couple of months to more than a year.

During the ca. 45 kyrs since the first Motuoapa eruption, the western parts of the pyroclastic cone underwent subsidence as a result of the tectonic evolution of the Taupo rift and of erosion. Only the lava capped parts of the tuff cone were preserved. At ca. 35 ka another eruption occurred in the vicinity of the earlier vent area, producing a small dacitic lava dome on the erosional remnant of the tuff cone. The tectonic activity affecting the area commenced during or after the second volcanic event, indicated by the formation of a graben transecting the dacite dome (Figs. 1 and 9). No contact was mapped between the Motuoapa succession and Oruanui Formation, but eruption ages are consistent with the established stratigraphic framework (Leonard et al, 2010). Lake terraces formed at multiple levels after the 232 AD Taupo eruption on the gentle sloping southern flanks of the peninsula, indicating the progressive lake level drop of Lake Taupo (Manville et al., 1999).

Conclusions

The examined volcanic succession of Motuoapa Peninsula exhibits a rare and relatively poorly understood style of explosive hydrovolcanic activity within the central TVZ. According to our study, explosive fragmentation mostly affected the outgassed part of magma, rendering magmatic gas-driven fragmentation ineffective. Based on the number of indirect evidences, such as particle vesicularity, thickness of pyroclastic deposits and cone morphology, and changes in eruptive styles, it is proposed that the eruption initiated in a subaqueous environment. The lowermost exposures most likely represent subaqueously emplaced coarse breccias that lack evidence of explosive fragmentation. As the volcanic materials piled up underwater, the top of the pile became sufficiently shallow and eruptions became more explosive forming a subaerial pyroclastic cone, comparable in size to typical tuff/pumice cones elsewhere. The middle-upper pyroclastic successions of Motuoapa Peninsula are dominated by coarse fall-dominated beds and PDC deposits produced by eruptions remarkably similar to Surtseyan-style eruptions. The late stage eruption style reverted to effusive, possibly coinciding with water no longer being able to access the vent.

The thick pyroclastic sequence and the total erupted volume of the rhyolitic succession indicate that prolonged subaqueous to emergent small-volume eruptions are also possible within the TVC besides the more common short-lived and highly energetic sub-Plinian to Plinian activity (Wilson, 1993). The explosivity of emergent activity strongly depends on the availability of water flowing into vent(s), the degree of interaction between magma and water, and the physical properties and vesiculation of magma, which make eruptions in lacustrine environments highly unpredictable.

U-Th zircon crystallization ages indicate that the magma reservoir that fed Motuoapa eruptions existed at least since ca. 140 ka and continuously produced zircon crystals for at least 100 kyrs. Overlapping (U-Th)/He zircon eruption ages of 77.2 ± 6.3 ka and 81.3 ± 9.2 ka obtained on two samples of the rhyolitic succession indicate that the volcanic activity occurred at ca. 80 ka. The eruption of dacite lava at ca. 35 ka, recorded by the (U-Th)/He zircon eruption age of 34.5 ± 3.1 ka represents a significantly younger event that occurred after substantial erosion of the pyroclastic cone.

Supplementary materials

Appendix 1: Secondary ionization mass spectrometry (SIMS) U–Th zircon results.

Acknowledgement

This research was supported by a Doctoral Scholarship of Institute of Agriculture and Environment, Massey University awarded to SK. MD was supported by the AuScope NCRIS2 program, Australian Research Council (ARC) Discovery funding scheme (DP160102427) and Curtin Research Fellowship. We thank Ermanno Brosch and other field assistants, Adam Frew for help with zircon dissolution, Bryant Ware for support with solution ICP-MS analyses, and I. Dunkl for sharing PepiFLEX software for ICP-MS data reduction. We thank Darren Gravley, Graham Leonard, and Pierre-Simon Ross for the suggestions on an early version of the manuscript. Finally, the authors thank editor Jose Luis Macias, and Natalia Pardo, James White and anonymous reviewer for constructive comments that improved the manuscript.

REFERENCES

Acocella, V., Spinks, K.D., Cole, J.W. and Nicol, A., 2003. Oblique back arc rifting of Taupo Volcanic zone, New Zealand. Tectonics, 22(4).

Agustin-Flores, J., Németh, K., Cronin, S.J., Lindsay, J.M. and Kereszturi, G., 2015. Construction of the North Head (Maungauika) tuff cone: a product of Surtseyan volcanism, rare in the Auckland Volcanic Field, New Zealand. Bulletin of Volcanology, 77(2): 17.

Anderson, S.W., Stofan, E.R., Plaut, J.J. and Crown, D.A., 1998. Block size distributions on silicic lava flow surfaces: implications for emplacement conditions. Geological Society of America Bulletin, 110(10): 1258-1267.

Barker, S.J., Wilson, C.J.N., Illsley-Kemp, F., Leonard, G.S., Mestel, E.R.H., Mauriohooho, K., Charlier, B.L.A. 2020. Taupō: an overview of New Zealand's youngest supervolcano, New Zealand Journal of Geology and Geophysics, DOI: 10.1080/00288306.2020.1792515.

Barker, S.J., Wilson, C.J.N., Smith, E.G., Charlier, B.L.A., Wooden, J.L., Hiess, J., Ireland, T.R. 2014. Post-supereruption magmatic reconstruction of Taupo volcano (New Zealand), as reflected in zircon ages and trace elements. Journal of Petrology, 55(8): 1511-1533.

Bibby, H.M., Risk, G.F., Macdonald, W.J.P. 1991. Resistivity survey of Motuoapa Springs, New Zealand. Proceedings 13th New Zealand Geothermal Workshop: 39-44.

Bignami, C. 2012. Handbook for volcanic risk management: Prevention, crisis management and resilience. In Handbook for volcanic risk management: Prevention, crisis management and resilience. MiaVita. Bureau de Recherches Géologiques et Minières.

Blott, S.J. and Pye, K., 2001. GRADISTAT: A grain size distribution and statistics package for the analysis of unconsolidated sediments. Earth Surface Processes and Landforms, 26(11): 1237-1248.

Bonnichsen, B. and Kauffman, D.F., 1987. Physical features of rhyolite lava flows in the Snake River Plain volcanic province, southwestern Idaho. Geological Society of America Special Papers, 212: 119-145.

Brown, S., Smith, R., Cole, J. and Houghton, B., 1994. Compositional and textural characteristics of the strombolian and surtseyan K-Trig basalts, Taupo Volcanic Centre, New Zealand: Implications for eruption dynamics. New Zealand Journal of Geology and Geophysics, 37(1): 113-126.

Brooker, M.R., Houghton, B.F., Wilson, C.J.N., Gamble, J.A. 1993. Pyroclastic phases of a rhyolitic dome building eruption - Puketarata tuff ring, Taupo Volcanic Zone, New Zealand. Bulletin of Volcanology. 55(6):395–406

Burgisser, A. and Gardner, J.E., 2004. Experimental constraints on degassing and permeability in volcanic conduit flow. Bulletin of Volcanology, 67(1): 42-56.

Büttner, R., Dellino, P., La Volpe, L., Lorenz, V. and Zimanowski, B., 2002. Thermohydraulic explosions in phreatomagmatic eruptions as evidenced by the comparison between pyroclasts and products from Molten Fuel Coolant Interaction experiments. Journal of Geophysical Research: Solid Earth (1978–2012), 107(B11): ECV 5-1-ECV 5-14.

Calder, E., Luckett, R., Sparks, R. and Voight, B., 2002. Mechanisms of lava dome instability and generation of rockfalls and pyroclastic flows at Soufriere Hills Volcano, Montserrat. Geological Society, London, Memoirs, 21(1): 173-190.

Carey, S., Sigurdsson, H., Mandeville, C. and Bronto, S., 1996. Pyroclastic flows and surges over water: an example from the 1883 Krakatau eruption. Bulletin of Volcanology, 57(7): 493-511.

Cas, R.A.F., Allen, R., Bull, S., Clifford, B. and Wright, J., 1990. Subaqueous, rhyolitic dome-top tuff cones: a model based on the Devonian Bunga Beds, southeastern Australia and a modern analogue. Bulletin of Volcanology, 52(3): 159-174.

Cas, R.A.F. and Wright, J.V., 1988. Volcanic successions modern and ancient: A geological approach to processes, products and successions. Chapman & Hall, London.

Charlier, B.L.A., Wilson, C.J.N., Lowenstern, J.B., Blake, S., Van Calsteren, P.W., Davidson, J.P. 2005. Magma generation at a large, hyperactive silicic volcano (Taupo, New Zealand) revealed by U–Th and U–Pb systematics in zircons. Journal of Petrology, *46*(1): 3-32.

Clarke, B., Calder, E. S., Dessalegn, F., Fontijn, K., Cortés, J. A., Naylor, M., ... and Yirgu, G. 2019. Fluidal pyroclasts reveal the intensity of peralkaline rhyolite pumice cone eruptions. Nature communications, 10(1), 1-10.

Cole, J.W., 1990. Structural control and origin of volcanism in the Taupo volcanic zone, New Zealand. Bulletin of Volcanology, 52(6): 445-459.

Cole, J. W., Milner, D. M., Spinks, K. D. 2005. Calderas and caldera structures: a review. Earth-Science Reviews, 69(1-2), 1-26.

Colombier, M., Scheu, B., Wadsworth, F. B., Cronin, S., Vasseur, J., Dobson, K. J., ... and Dingwell, B. D. 2018. Vesiculation and Quenching During Surtseyan Eruptions at Hunga Tonga-Hunga Ha'apai Volcano, Tonga. Journal of Geophysical Research: Solid Earth, 123(5), 3762-3779.

Cousens, B.L., Clague, D.A. and Sharp, W.D., 2003. Chronology, chemistry, and origin of trachytes from Hualalai Volcano, Hawaii. Geochemistry Geophysics Geosystems, 4.

Danišík, M., Schmitt, A. K., Stockli, D. F., Lovera, O. M., Dunkl, I., Evans, N. J., 2017. Application of combined U-Th-disequilibrium/U-Pb and (U-Th)/He zircon dating to tephrochronology. Quaternary Geochronology, 40, 23-32.

Danišík, M., Shane, P., Schmitt, A.K., Hogg, A., Santos, G.M., Storm, S., Evans, N.J., Fifield, L.K. and Lindsay, J.M., 2012. Re-anchoring the late Pleistocene tephrochronology of New Zealand based on concordant radiocarbon ages and combined 238 U/230 Th disequilibrium and (U–Th)/He zircon ages. Earth and Planetary Science Letters, 349: 240-250.

Danišík, M., Lowe, D.J., Schmitt, A.K., Friedrichs, B., Hogg, A.G. and Evans, N.J., 2020. Sub-millennial eruptive recurrence in the silicic Mangaone Subgroup tephra sequence, New Zealand, from Bayesian modelling of zircon double-dating and radiocarbon ages. Quaternary Science Reviews, 246, p.106517.

Davey, F., Henrys, S. and Lodolo, E., 1995. Asymmetric rifting in a continental back-arc environment, North Island, New Zealand. Journal of Volcanology and Geothermal Research, 68(1): 209-238.

Davy, B. and Caldwell, T., 1998. Gravity, magnetic and seismic surveys of the caldera complex, Lake Taupo, North Island, New Zealand. Journal of Volcanology and Geothermal Research, 81(1): 69-89.

Dellino, P. and La Volpe, L., 1995. Fragmentation versus transportation mechanisms in the pyroclastic sequence of Monte Pilato-Rocche Rosse (Lipari, Italy). Journal of Volcanology and Geothermal Research, 64(3-4): 211-231.

Doronzo, D. M. 2012. Two new end members of pyroclastic density currents: forced convection-dominated and inertia-dominated. Journal of Volcanology and Geothermal Research, 219, 87-91.

Doronzo, D. M., Valentine, G. A., Dellino, P., de Tullio, M. D. 2010. Numerical analysis of the effect of topography on deposition from dilute pyroclastic density currents. Earth and Planetary Science Letters, 300(1-2), 164-173.

Duraiswami, R. A., Jutzeler, M., Karve, A. V., Gadpallu, P., Kale, M. G., 2019. Subaqueous effusive and explosive phases of late Deccan volcanism: evidence from Mumbai Islands, India. Arabian Journal of Geosciences, 12(23), 703.

Ehlers, T.A. and Farley, K.A. 2003. Apatite (U–Th)/He thermochronometry: methods and applications to problems in tectonic and surface processes. Earth and Planetary Science Letters, 2*06*(1-2): 1-14.

Ewart, A., Hildreth, W. and Carmichael, I.S., 1975. Quaternary acid magma in New Zealand. Contributions to Mineralogy and Petrology, 51(1): 1-27.

Farley, K.A., Kohn, B.P., Pillans, B., 2002. The effects of secular disequilibrium on (U–Th)/He systematics and dating of Quaternary volcanic zircon and apatite. Earth and Planetary Science Letters 201 (1): 117–125.

Farley, K., Wolf, R. and Silver, L., 1996. The effects of long alpha-stopping distances on (U・ Th)/He ages. Geochimica et cosmochimica acta, 60(21): 4223-4229.

Fink, J.H. and Anderson, S.W., 2017. Emplacement of Holocene silicic lava flows and domes at Newberry, South Sister, and Medicine Lake volcanoes, California and Oregon. 2328-0328, US Geological Survey.

Fink, J. H., Anderson, S. W., Manley, C. R. 1992. Textural constraints on effusive silicic volcanism: Beyond the permeable foam model. Journal of Geophysical Research: Solid Earth, 97(B6), 9073-9083.

Freundt, A., 2003. Entrance of hot pyroclastic flows into the sea: experimental observations. Bulletin of Volcanology, 65(2-3): 144-164.

Friedrichs, B., Schmitt, A.K., McGee, L., and Turner, S., 2020. U-Th whole rock data and high spatial resolution U-Th disequilibrium and U-Pb zircon ages of Mt. Erciyes and Mt. Hasan Quaternary stratovolcanic complexes (Central Anatolia). Data Br. 29. https://doi.org/10.1016/j.dib.2020.105113

Giachetti, T., Druitt, T.H., Burgisser, A., Arbaret, L. and Galven, C., 2010. Bubble nucleation, growth and coalescence during the 1997 Vulcanian explosions of Soufrière Hills Volcano, Montserrat. Journal of Volcanology and Geothermal Research, 193(3-4): 215-231.

Graettinger, A. H. and Valentine, G. A. 2017. Evidence for the relative depths and energies of phreatomagmatic explosions recorded in tephra rings. Bulletin of Volcanology, 79(12), 88.

Graettinger, A. H., Valentine, G. A., Sonder, I., Ross, P. S., White, J. D. 2015. Facies distribution of ejecta in analog tephra rings from experiments with single and multiple subsurface explosions. Bulletin of Volcanology, 77(8), 66.

Gravley, D., Deering, C., Leonard, G. and Rowland, J., 2016. Ignimbrite flare-ups and their drivers: A New Zealand perspective. Earth-Science Reviews, 162: 65-82.

Gravley, D.M., 2004. The Ohakuri pyroclastic deposits and the evolution of the Rotorua-Ohakuri volcanotectonic depression, Unpublished PhD thesis, Canterbury University, Christchurch, 227 pp.

Heiken, G., 1972. Morphology and petrography of volcanic ashes. Geological Society of America Bulletin, 83(7): 1961-1988.

Heiken, G. and Wohletz, K., 1987. Tephra deposits associated with silicic domes and lava flows. Geological Society of America Special Papers, 212: 55-76.

Hetényi, G., Taisne, B., Garel, F., Médard, É., Bosshard, S. and Mattsson, H.B., 2012. Scales of columnar jointing in igneous rocks: field measurements and controlling factors. Bulletin of Volcanology, 74(2): 457-482.

Houghton, B.F., Weaver, S.D., Wilson, C.J.N. and Lanphere, M.A., 1992. Evolution of a quaternary peralkaline volcano - Mayor Island, New Zealand. Journal of Volcanology and Geothermal Research, 51(3): 217-236.

Houghton, B.F., Wilson, C.J.N. and Weaver, S., 1987. The Opo Bay Tuff cone, Mayor Island. Interaction between rising gas-poor pantelleritic magma and external water.

Houghton, B.F. and Wilson, C.J.N., 1989. A vesicularity index for pyroclastic deposits. Bulletin of Volcanology, 51(6): 451-462.

Jensen, R.A., Donnelly-Nolan, J.M. and Mckay, D., 2009. A field guide to Newberry Volcano, Oregon. Field Guides, 15: 53-79.

Jurado-Chichay, Z. and Walker, G., 2000. Stratigraphy and dispersal of the Mangaone Subgroup pyroclastic deposits, Okataina volcanic centre, New Zealand. Journal of Volcanology and Geothermal Research, 104(1): 319-380.

Kobayashi, T., 1982. Geology of Sakurajima Volcano: a review. Bulletin of the Volcanological Society of Japan, 27: 277-292.

Kobayashi, T., Nairn, I., Smith, V. and Shane, P., 2005. Proximal stratigraphy and event sequence of the c. 5600 cal. yr BP Whakatane rhyolite eruption episode from Haroharo volcano, Okataina Volcanic Centre, New Zealand. New Zealand Journal of Geology and Geophysics, 48(3): 471-490.

Kokelaar, B.P., 1983. The mechanism of Surtseyan volcanism. Journal of the Geological Society, 140(6): 939-944.

Kokelaar, B.P., 1986. Magma-water interactions in subaqueous and emergent basaltic volcanism. Bulletin of Volcanology, 48(5): 275-289.

Kósik, S., 2018. Small-volume volcanism associated with polygenetic volcanoes, Taupo Volcanic Zone, New Zealand, Unpublished PhD thesis, Massey University, Palmerston North, 304 pp.

Kósik, S., Bebbington, M.S., Németh, K., 2020. Spatio-temporal hazard estimation in the central silicic part of Taupo Volcanic Zone, New Zealand, based on small to medium volume eruptions. Bulletin of Volcanology, 82:50.

Kósik, S., Németh, K., Lexa, J. and Procter, J.N., 2019. Understanding the evolution of a small-volume silicic fissure eruption: Puketerata Volcanic Complex, Taupo Volcanic Zone, New Zealand. Journal of Volcanology and Geothermal Research, 383: 28-46.

Kósik, S., Németh, K., Procter, J.N. and Bebbington, M.S., 2017. Hazard implications of silicic small-volume volcanism within the Taupo Volcanic Zone, New Zealand: spatial, temporal, volumetric and eruptive style distribution of the eruptive vents, IAVCEI 2017 Scientific Assembly - Fostering Integrative Studies of Volcanism, Portland, Oregon, USA.

Leonard G.S., Begg J.G.,Wilson C.J.N. 2010. Geology of the Rotorua area. Institute of Geological and Nuclear Sciences 1:250,000 geological map 5. Sheet + 102 p. Lower Hutt, New Zealand, GNS Science

Lexa, J., Seghedi, I., Németh, K., Szakacs, A., Konecny, V., Pecskay, Z., Fueloep, A. and Kovacs, M., 2010. Neogene-Quaternary Volcanic forms in the Carpathian-Pannonian Region: a review. Central European Journal of Geosciences, 2(3): 207-U275.

Lipman, P. W. 1997. Subsidence of ash-flow calderas: relation to caldera size and magma-chamber geometry. Bulletin of volcanology, 59(3), 198-218.

Ludwig, K.R., 2012. User’s manual for isoplot 3.75–4.15. Berkeley Geochronology Center.

Mahon, W.A.J. and Klyen L.E., 1968. Chemistry of the Tokaanu-Waihi hydrothermal area. New Zealand Journal of Science, 11: 140-150.

Manville, V., 2010. An overview of break-out floods from intracaldera lakes. Global and Planetary Change, 70(1): 14-23.

Manville, V., Segschneider, B., Newton, E., White, J.D.L., Houghton, B.F. and Wilson, C.J.N., 2009. Environmental impact of the 1.8 ka Taupo eruption, New Zealand: Landscape responses to a large-scale explosive rhyolite eruption. Sedimentary Geology, 220(3-4): 318-336.

Manville, V., White, J.D.L., Houghton, B.F., Wilson, C.J.N., 1999. Paleohydrology and sedimentology of a post–1.8 ka breakout flood from intracaldera Lake Taupo, North Island, New Zealand. Geological Society of America Bulletin, 111(10): 1435-1447.

Manville V., Wilson C.J.N. 2004. The 26.5 ka Oruanui eruption,New Zealand: a review of the roles of volcanism and climate in the sedimentary response. New Zealand Journal of Geology and Geophysics, 47:525–547

McClintock, M. and White, J.D.L., 2006. Large phreatomagmatic vent complex at Coombs Hills, Antarctica: wet, explosive initiation of flood basalt volcanism in the Ferrar-Karoo LIP. Bulletin of Volcanology, 68(3), 215-239.

Mongrain, J., Larsen, J.F. and King, P., 2008. Rapid water exsolution, degassing, and bubble collapse observed experimentally in K-phonolite melts. Journal of Volcanology and Geothermal Research, 173(3-4): 178-184.

Mortimer, N., and Scott, J.M. 2020. Volcanoes of Zealandia and the Southwest Pacific. New Zealand Journal of Geology and Geophysics 63(4), 1-7.

Mueller, W. and White, J.D., 1992. Felsic fire-fountaining beneath Archean seas: pyroclastic deposits of the 2730 Ma Hunter Mine Group, Quebec, Canada. Journal of Volcanology and Geothermal Research, 54(1-2): 117-134.

Murch, A. P., White, J. D. L., & Carey, R. J., 2019. Unusual fluidal behavior of a silicic magma during fragmentation in a deep subaqueous eruption, Havre volcano, southwestern Pacific Ocean. Geology, 47(5), 487-490.

Murgulov, V., Luketina, K., Zarrouk, S., 2016. Investigation of the geothermal signature of the Motuoapa marina, Lake Taupo, New Zealand. Proceedings 38th New Zealand Geothermal Workshop

Nairn, I.A., 2002. Geology of the Okataina Volcanic Centre, scale 1: 50 000. Institute of Geological and Nuclear Sciences geological map 25. 1 sheet+ 156 p. Institute of Geological and Nuclear Sciences, Lower Hutt, New Zealand.

Németh, K. and Kósik, S., 2020a. Review of explosive hydrovolcanism. Geosciences, 10(2): 44.

Németh, K. and Kósik, S., 2020b. The role of hydrovolcanism in the formation of the Cenozoic monogenetic volcanic fields of Zealandia, New Zealand Journal ofGeology and Geophysics, 63:4, 402-427.

Noguchi, S., Toramaru, A. and Shimano, T., 2006. Crystallization of microlites and degassing during magma ascent: constraints on the fluid mechanical behavior of magma during the Tenjo Eruption on Kozu Island, Japan. Bulletin of Volcanology, 68(5): 432-449.

Orsi, G., Ruvo, L. and Scarpati, C., 1989. The Serra della Fastuca Tephra at Pantelleria: physical parameters for an explosive eruption of peralkaline magma. Journal of Volcanology and Geothermal Research, 39(1): 55-60.

Reyners, M., 2013. The central role of the Hikurangi Plateau in the Cenozoic tectonics of New Zealand and the Southwest Pacific. Earth and Planetary Science Letters, 361: 460-468.

Reynolds, M.A., 1980. 1953-57 eruption of Tuluman volcano: Rhyolitic volcanic activity in the northern Bismarck Sea. Geological Survey of Papua New Guinea.

Ross, P.-S., Núñez, G.C. and Hayman, P., 2017. Felsic maar-diatreme volcanoes: a review. Bulletin of Volcanology, 79(2): 20.

Ross, P.-S., and White, J.D.L., 2006. Debris jets in continental phreatomagmatic volcanoes: a field study of their subterranean deposits in the Coombs Hills vent complex, Antarctica. Journal of Volcanology and Geothermal Research, 149(1-2), 62-84.

Rowland, J.V., Wilson, C.J.N. and Gravley, D.M., 2010. Spatial and temporal variations in magma-assisted rifting, Taupo Volcanic Zone, New Zealand. Journal of Volcanology and Geothermal Research, 190(1-2): 89-108.

Sakata, S., Hirakawa, S., Iwano, H., Danhara, T., Guillong, M., Hirata, T., 2017. A new approach for constraining the magnitude of initial disequilibrium in Quaternary zircons by coupled uranium and thorium decay series dating. Quaternary Geochronology, 38: 1-12.

Schmitt, A.K., Danišík, M., Evans, N.J., Siebel, W., Kiemele, E., Aydin, F. and Harvey, J.C., 2011. Acigöl rhyolite field, Central Anatolia (part 1): high-resolution dating of eruption episodes and zircon growth rates. Contributions to Mineralogy and Petrology, 162(6): 1215-1231.

Schmitt, A.K., Stockli, D.F., Lindsay, J.M., Robertson, R., Lovera, O.M. and Kislitsyn, R., 2010. Episodic growth and homogenization of plutonic roots in arc volcanoes from combined U–Th and (U–Th)/He zircon dating. Earth and Planetary Science Letters, 295(1-2): 91-103.

Scott, C. R., Richard, D., Fowler, A. D. 2003. An Archean submarine pyroclastic flow due to submarine dome collapse: the Hurd Deposit, Harker Township, Ontario, Canada. In White, J.D.L., Smellie, J.L., Clague, D.A. (Eds) Explosive subaqueous volcanism. Geophysical Monograph, 140: 317-327.

Shea, T., Leonhardi, T., Giachetti, T., Lindoo, A., Larsen, J., Sinton, J. and Parsons, E., 2017. Dynamics of an unusual cone-building trachyte eruption at Pu ‘u Wa ‘awa ‘a, Hualālai volcano, Hawai ‘i. Bulletin of Volcanology, 79(4): 26.

Sheridan, M.F. and Wohletz, K.H., 1983. Hydrovolcanism: basic considerations and review. Journal of Volcanology and Geothermal Research, 17(1-4): 1-29.

Smith, R.T., 1998. Eruptive and depositional models for units 3 and 4 of the 1.85 ka Taupo eruption: Implications for the nature of large-scale'wet'eruptions, Unpublished PhD Thesis, University of Canterbury, Christchurch.

Smith, R.T. and Houghton, B.F., 1995. Delayed deposition of plinian pumice during phreatoplinian volcanism: the 1800-yr-BP Taupo eruption, New Zealand. Journal of Volcanology and Geothermal Research, 67(4): 221-226.

Spinks, K.D., Acocella, V., Cole, J.W. and Bassett, K.N., 2005. Structural control of volcanism and caldera development in the transtensional Taupo Volcanic Zone, New Zealand. Journal of Volcanology and Geothermal Research, 144(1): 7-22.

Sutton, A.N., Blake, S. and Wilson, C.J.N., 1995. An outline geochemistry of rhyolite eruptives from Taupo volcanic centre, New Zealand. Journal of Volcanology and Geothermal Research, 68(1-3): 153-175.

Tilling, R. I. 1989. Volcanic hazards and their mitigation: progress and problems. Reviews of Geophysics, 27(2), 237-269

Tuffen, H., James, M.R., Castro, J.M., Schipper, C.I., 2013. Exceptional mobility of an advancing rhyolitic obsidian flow at Cordón Caulle volcano in Chile. Nature Communications, *4*(1): 1-7.

Valentine, G. A., Graettinger, A. H., Macorps, É., Ross, P. S., White, J. D., Döhring, E., Sonder, I. 2015. Experiments with vertically and laterally migrating subsurface explosions with applications to the geology of phreatomagmatic and hydrothermal explosion craters and diatremes. Bulletin of Volcanology, 77(3), 15.

Valentine, G.A., White, J.D.L., Ross, P.-S., Graettinger, A.H., Sonder, I., 2017. Updates to Concepts on Phreatomagmatic Maar-Diatremes and Their Pyroclastic Deposits. Frontiers in Earth Science. 5.

Vandergoes, M.J., Hogg, A.G., Lowe, D.J., Newnham, R.M., Denton, G.H., Southon, J., Barrell, D.J.A., Wilson, C.J.N., McGlone, M.S., Allan, A.S.R., Almond, P.C., Petchey, F., Dabell, K., Dieffenbacher-Krall, A.C. and Blaauw, M., 2013. A revised age for the Kawakawa/Oruanui tephra, a key marker for the Last Glacial Maximum in New Zealand. Quaternary Science Reviews, 74: 195-201.

van Otterloo, J., Cas, R. A., Scutter, C. R. 2015. The fracture behaviour of volcanic glass and relevance to quench fragmentation during formation of hyaloclastite and phreatomagmatism. Earth-Science Reviews, 151, 79-116.

Verwoerd, W. and Chevallier, L., 1987. Contrasting types of surtseyan tuff cones on Marion and Prince Edward islands, southwest Indian Ocean. Bulletin of Volcanology, 49(1): 399-413.

von Lichtan, I., White, J.D.L., Manville, V. and Ohneiser, C., 2016. Giant rafted pumice blocks from the most recent eruption of Taupo volcano, New Zealand: Insights from palaeomagnetic and textural data. Journal of Volcanology and Geothermal Research, 318: 73-88.

Walker, G. P. 1984. Downsag calderas, ring faults, caldera sizes, and incremental caldera growth. Journal of Geophysical Research: Solid Earth, 89(B10), 8407-8416.

Wallace, L.M., Beavan, J., McCaffrey, R. and Darby, D., 2004. Subduction zone coupling and tectonic block rotations in the North Island, New Zealand. Journal of Geophysical Research: Solid Earth, 109(B12).

White, J. D. L. and Houghton, B.F. 2000. Surtseyan and related phreatomagmatic eruptions. In. Sigurdsson, H., Houghton, B., McNutt, S., Rymer, H., & Stix, J. (Eds.) Encyclopedia of volcanoes. Academic Press, San Diego, 495-513.

White, J. D. L. and Houghton, B.F. 2006. Primary volcaniclastic rocks. Geology, 34(8), 677-680.

White, J.D.L, Smellie, J.L. and Clague, D.A., 2003. Introduction: A deductive outline and topical overview of subaqueous explosive volcanism. In White, J.D.L., Smellie, J.L., Clague, D.A. (Eds) Explosive subaqueous volcanism. Geophysical Monograph, 140: 1-23.

White, J.D.L. and Ross, P.-S., 2011. Maar-diatreme volcanoes: A review. Journal of Volcanology and Geothermal Research, 201(1-4): 1-29.

Wilson, C.J.N., 1993. Stratigraphy, chronology, styles and dynamics of late Quaternary eruptions from Taupo volcano, New Zealand. Philosophical Transactions of the Royal Society of London A: Mathematical, Physical and Engineering Sciences, 343(1668): 205-306.

Wilson, C.J.N., 2001. The 26.5 ka Oruanui eruption, New Zealand: an introduction and overview. Journal of Volcanology and Geothermal Research, 112(1-4): 133-174.

Wilson, C.J.N. and Charlier, B.L.A., 2016. The life and times of silicic volcanic systems. Elements, 12(2): 103-108.

Wilson, C.J.N. and Walker, G.P., 1985. The Taupo eruption, New Zealand I. General aspects. Philosophical Transactions of the Royal Society of London A: Mathematical, Physical and Engineering Sciences, 314(1529): 199-228.

Wilson, C.J.N., Gravley, D.M., Leonard, G.S. and Rowland, J.V., 2009. Volcanism in the central Taupo Volcanic Zone, New Zealand: tempo, styles and controls. Studies in Volcanology: The Legacy of George Walker. Special Publications of IAVCEI, 2: 225-247.

Wilson, C.J.N., Houghton, B.F., McWilliams, M.O., Lanphere, M.A., Weaver, S.D. and Briggs, R.M., 1995. Volcanic and structural evolution of Taupo Volcanic Zone, New Zealand: a review. Journal of Volcanology and Geothermal Research, 68(1-3): 1-28.

Wilson, C.J.N., Rogan, A.M., Smith, I.E.M., Northey, D.J., Nairn, I.A. and Houghton, B.F., 1984. Caldera volcanos of the Taupo Volcanic Zone, New Zealand. Journal of Geophysical Research, 89(NB10): 8463-8484.

Wohletz, K.H. and Sheridan, M.F., 1983. Hydrovolcanic explosions II. Evolution of basaltic tuff rings and tuff cones. American Journal of Science, 283(5): 385-413.

Wright, H.M., Cashman, K.V., Rosi, M. and Cioni, R., 2007. Breadcrust bombs as indicators of Vulcanian eruption dynamics at Guagua Pichincha volcano, Ecuador. Bulletin of Volcanology, 69(3): 281-300.

Yokoyama, I., 2005. Growth rates of lava domes with respect to viscosity of magmas. Annals of Geophysics, 48(6).

Figure captions

Fig. 1 Right panel – Geomorphology and geology of Motuoapa Peninsula as indicated by a slope map with shaded relief DEM layer as a background, data source: (1 m resolution LiDAR DEM Waikato Regional Council and Aerial Mapping Ltd., 2006). Map shows sampling locations and the main *stratigraphic units: a – pyroclastic sequence relating to the eruption of rhyolitic magma; b – brecciated or coherent rhyolitic lava; and c – coherent dacite lava. Red dots in the squares of sampling sites indicate samples that were used for geochronology. The regional map (inset map a) shows the geographic position of Lake Taupo and the TVZ with mentioned volcanic centres; 1 – Taupo, 2 – Rotorua, 3 – Okataina within the North Island and its relative position to the plate boundary. Inset map b indicates the location of the study area relative to Lake Taupo.*

Fig. 2 SEM images of variably vesicular ash particles (a-c) with quenching cracks (c, yellow arrows) and microscopic image of well-cemented lapilli tuff containing lapilli fragments displaying highly vesicular inflated cores and vesicle-free chilled rinds (d, red arrows).

Fig. 3 Envelope density of pyroclastic samples. Red dashed lines indicate the average envelope density of the samples

Fig. 4 Representative pyroclastic sequences of the Motuoapa Peninsula. a – shows lithofacies Ex-3, which consists of heterogeneous tuff-breccia containing blocks of stratified lapilli tuff that have been emplaced into the heterogeneous matrix from the nearby crater rim (loc. P3, Fig. 1); b – The upper part of the image shows blocks of matrix-supported lapilli tuff (A-bed) alternating with clast supported, poorly stratified lapilli tuff (L-bed). These tuff beds are representative of lithofacies Ex-2 emplaced into the heterogeneous tuff-breccia. Together these lithologies make up lithofacies Ex-3); c – Heterogeneous, clast-supported, non-stratified tuff-breccia of Ex-3 lithofacies with variable discolouration; d – Poorly-sorted, clast-supported tuff-breccia of lithofacies Ex-1 (loc. 2-02, Fig. 1); e – Normal-graded, poorly-sorted, clast-supported breccia enclosed by non-graded, matrix-supported lapilli tuff in lithofacies Ex-1 (loc. 2-02, Fig. 1); f – Matrix-supported weakly-stratified tuff-breccia of lithofacies Ex-1 (loc. P6, Fig. 1); g – ~100 m thick sequence of lithofacies Ex-2 (loc. P5, Fig. 1); h – Poorly-sorted, in places stratified lapilli tuff of lithofacies Ex-2 from locality 2-05 (Fig. 1); the insert shows the grain size distribution (MD mean diameter; σ=sorting); i-j – show lithofacies Ex-2 present at lower stratigraphic levels with clast-supported L-beds and thin A-beds (loc. 3-09, Fig. 1); k-l – show lithofacies Ex-2 at higher stratigraphic levels with more pronounced and thicker A-beds (loc. P5, Fig. 1) (see also Fig. 8e).

Fig. 5 Grain size distribution of L-beds (MOT2-01, MOT2-05, MOT3-09) compared to representative granulometric data of common beds identified in other small-volume volcanoes considered to be formed in explosive hydrovolcanism including shallow Surtseyan and maar forming eruptions from the Auckland Volcanic Field (AVF) and Puketerata Volcanic Complex, New Zealand. NH-6 represents a fall-dominated unit of a Surtseyan eruption of North Head volcano, AVF (Agustin-Flores et al., 2015), PUK3-

26L (proximal fall), PUK4-21I (proximal diluted PDC), PUK3 24A (medial diluted PDC), and PUK4 21E (proximal PDC) are from the silicic Puketerata maar-dome complex, Taupo Volcanic Zone (Kósik et al., 2019).

Fig. 6 Representative outcrops of lava lithofacies of Motuoapa Peninsula. a – The contact between the pyroclastic succession of Ex-2 lithofacies (1) and vertically-jointed coherent lava, Ef-1 lithofacies (2); b-c – Vertically-jointed coherent rhyolite lava (loc. P4, Fig. 1); d – Flow-banded, coherent rhyolite lava (loc. P2, Fig. 1); e-h – Lava breccia displaying different degrees of autofragmentation (loc. P1, Fig. 1).

Fig. 7 Zircon U-Th (blue squares) and (U-Th)/He ages (red diamonds) with 1σ analytical uncertainties displayed in ranked order plots. The eruption ages and their uncertainties (95% confidence interval) calculated as weighted average of (U-Th)/He ages are listed next to the sample code and displayed as vertical dashed orange lines and yellow rectangles. Kernel density and probability density function curves for zircon U-Th ages (green dashed and dotted lines, respectively) were constructed by DensityPlotter (Vermeesch, 2012). MSWD: mean square weighted deviation for (U-Th)/He data. For clarity, only ages <180 ka are displayed, the full dataset can be found in Appendix 1. Note that U-Th and (U-Th)/He ages of sample MO-3 are significantly younger than those of samples MO-1 and MO-2.

Fig. 8 Deposits relating to various hydrovolcanic explosive eruptions in New Zealand; a –Medial succession of the silicic Puketerata Volcanic Complex (Kósik et al., 2019) with wet and dry surge deposits with bomb sags (BS) alternating with major fall (F1, F2) or thin shower beds, b – Medial sequence of the 232 AD Taupo eruption at 38.748°S 176.200°E; c – Structure of the phreatoplinian Rotongaio ash member of Taupo Pumice Formation. The phreatoplinian beds of Taupo dominantly encompasses poorly sorted pumice and accretionary lapilli-bearing, vesicular, fine ash-dominated beds (Hatepe ash; MD: 3.3-5.1, σ: 1.9-3.8) and beds of poorly to non-vesicular juvenile fragments dominated by extremely fine ash with common mud lumps and soft-sediment deformation (Rotongaio ash; MD: -1.1-5.5, σ: 0.9-4.2) (Smith, 1998). Both of these units consist of multiple layers of fallout and proximally wet, cohesive pyroclastic density current deposits (Smith, 1998), d – Pyroclastic sequence of the Surtseyan tuff cone of North Head volcano, AVF (Agustin-Flores et al., 2015), e – Pyroclastic sequence at higher stratigraphic levels of Motuoapa Peninsula with ash-dominated (A), lapilli-dominated (L) units and angular ballistic bombs (b).

Fig. 9 Stratigraphy and structure of the Motuoapa Peninsula indicated on a 1 m LiDAR DEM (not to scale). The cliff's height near the inferred vent is about 100m. Orange arrows indicate flow directions of lava; fault lines are indicated by white dashed lines. Red arrows indicate the sampling locations for geochronology.